Research Article

Aditya Rio Prabowo*, Jung Min Sohn, Dong Myung Bae, and Joung Hyung Cho

Performance assessment on a variety of double side structure during collision interaction with other ship

https://doi.org/10.1515/cls-2017-0017
Received Apr 30, 2017; accepted Jun 14, 2017

Abstract: The main goal of the present paper was to study the physical response of a double side skin (DSS) structure under impact load in a collision event between two ships. Collision energy and damage extent (size and location) during the collision process were observed together with damage patterns on side structure. The ships were modeled after a Ro-Ro passenger ship and cargo reefer which were involved in a ship collision on the Sunda Strait while the analyses were performed using non-linear simulations FEM to produce virtual simulation data. Several cases were proposed to be investigated in this work with involvement of parameters *i.e.* penetration location and ship materials which were embedded on the structure model. A series of material experiments and testing was conducted to obtain detailed material properties which were to be deployed in simulation. It was shown that, after penetration at the transition location, the striking ship was successfully deforming and forming tears to the inner skin. On the other hand, with identical structure and identical mass of construction, the use of high-strength low-alloy (HSLA) steel as the repair material offered considerably better capacity in absorbing the impact load than plain-carbon steel.

Keywords: Ship-ship collision; field survey; material testing; virtual experiment; double side skin (DSS); collision energy; damage characteristic

***Corresponding Author: Aditya Rio Prabowo:** Interdisciplinary Program of Marine Convergence Design, Pukyong National University, Republic of Korea; Department of Naval Architecture and Marine Systems Engineering, Pukyong National University, Republic of Korea; Email: aditya@pukyong.ac.kr; Tel.: +82 51 629 6613; Fax.: +82 51 629 6608

Jung Min Sohn, Dong Myung Bae: Department of Naval Architecture and Marine Systems Engineering, Pukyong National University, Republic of Korea

Joung Hyung Cho: Interdisciplinary Program of Marine Convergence Design, Pukyong National University, Republic of Korea

1 Introduction

According to the Oil Pollution Act 1990 (OPA 90) and equivalent International Maritime Organization (IMO), requirements must be satisfied in the structural design of ships carrying dangerous or pollutant cargoes, for example chemicals, bulk oil, liquefied gas to reduce the possibility and amount of environmental disaster as presented in Figure 1. The safety of merchant shipping and passenger vessels also needs to be taken seriously in order to avoid a costly repair process (Figure 2) and the same tragedy such as befell the Titanic approximately a century ago. The primary requirements are including the arrangement of a double bottom with a required minimum height and double sides with a required minimum width. In this context, to reduce the casualties in a ship collision and grounding accident, both of OPA 90 and IMO require that the minimum vertical height, h, of each double bottom ballast tank or void is not less than 2.0 m or B/15 with B is ship's beam, whichever is the lesser, but in no case is the height to be less than 1.0 m. OPA and IMO also require that the minimum width, w, of each wing ballast tank or void space is not to be less than 0.5+DWT/20,000 (m) or w equals 2.0 m, whichever is the lesser, where DWT is the deadweight of the ship in tonnes. In no case, w is to be less than 1.0 m [1]. After applying the requirement, several methods, such as analytical formula [2] can be considered to assess the designed double hull

Safety of the cargoes or in this case the trading commodities have to be ensured in the distribution process. However accidents such as already mentioned above, collision and grounding always have possibility to take place in various scenarios, including with numerous objects as discussed by in collision between ship and jack-up [4], ice-steel interaction [5] and combined-load situation which affect its reliability [6]. The behaviour of ship structures specifically the side skin needs to be analysed since the breach of the side skin is one of the important parameters in safety, not only to the ship but also passenger, cargo and environment.

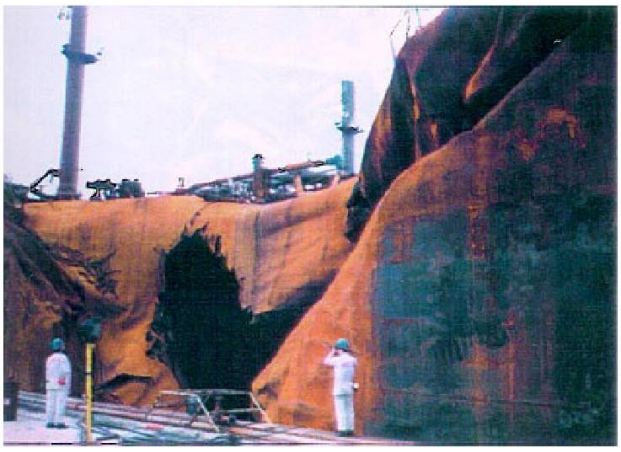

Figure 1: Damage in collision accident caused 10,000 tons oil was spilled [3].

Figure 2: Repair process of side structure after a collision incident.

The present paper is addressed to investigate the response of a ship's side structure subjected to an accidental load of collision between two ships. Different widths of double side skin are introduced to be observed as the main subject while the location of contact points of two involved ships and implemented materials which deploys various materials with different mechanical properties on a structural model are taken as independent variables.

2 Concept of impact phenomenon

The fundamental concept of collision and grounding assessment has been introduced and developed up to today. A study on 26 collision cases of full-scale ship accidents was performed by Minorsky [7] and the empirical formula method of predicting and analyzing began from this

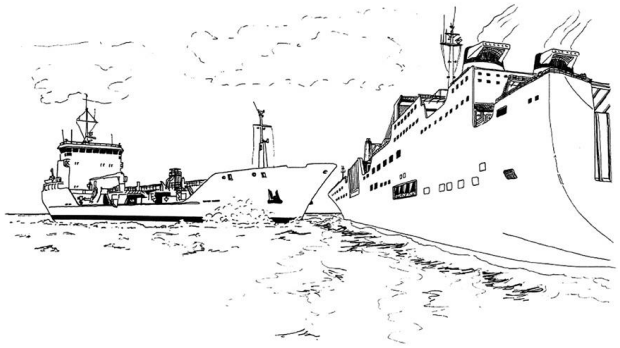

Figure 3: Collision between two ships [13].

point. The high-energy collision formula by Minorsky then was improved by Vaughan [8], Woisin [9] and Zhang [3] in a period of time spanning approximately 40 years. Other methods in predicting impact influence on a ship's structure are also performed by actual experiments. Several experiments on ship collisions have been carried out since the early 1960s. From 1962 to 1976, investigators in Italy, Germany and Japan conducted a series of model tests which were concerned with the design of nuclear powered ships protecting the nuclear reactors from collision damage. Previous researchers have given detailed reviews on these experiments, for example Jones [10], Amdahl [11], Samuelides and Frieze [12] and Pedersen *et al.* [13]. Since the full-scale or model tests are considered costly in terms of time and money, the experiment involving material can be considered a good alternative to boost the similarities between the model and results from numerical analyses which will be introduced in the next paragraphs.

In side collisions (Figure 3), Minorsky and Zhang described the analytical theory of this phenomenon. In this theory, the two objects *i.e.* involved ships are divided into two classes, the first is the striking ship and the second is the struck ship. The striking ship is introduced as the object which strikes the other object. In a ship collision process, this object penetrates into the other ship's structure. The struck ship is the other ship's structure in the previous statement which gets penetrated by the striking body. An illustration of these ships is presented in Figures 4 and 5. The angle formed by two ships during the collision process is represented by β or collision angle. Even though this theory is a simplified form due to the limitless possibility and scenario causing ship collision, the coordinate systems can be considered a good estimation in assessment.

In the last two decades, the human race has undergone significant development especially in computational technology. This technology has been applied to many as-

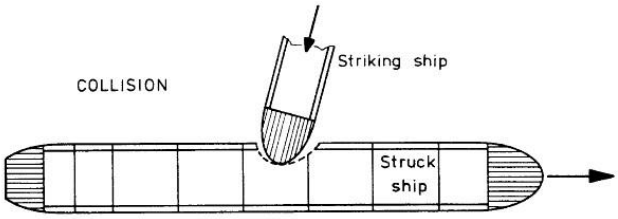

Figure 4: Side collision by upper view [14].

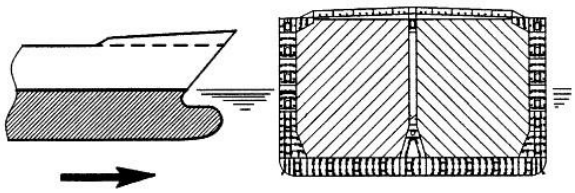

Figure 5: Side collision on perspective of front view [14].

Figure 6: Destroyed material: medium-carbon steel 1030.

Figure 7: Repair material: steel grade AH36.

pects of human life, such as transportation, production as well as calculation and measurement fields. In engineering itself, the aspects of calculation and measurement itself hold a vital role as the prediction of behaviour and characteristics of an observed object can be performed with virtual simulation. The simulation can be considered as an alternative way to solve engineering problems since the failure probability and cost of some real experiment cases cannot be controlled and can be too immense. The application of the virtual simulation is also deployed in naval architecture, marine and ocean engineering to assess some physical phenomenon. In collision analysis [15–17], finite element method (FEM) approach can be considered as a popular method. In FEM analysis, there are two methodologies that exist to solve engineering problem based on their types. These methodologies are namely, implicit and explicit techniques. In numerical calculation, matrix inversion is the more computationally expensive operation. Implicit methodology introduces the method where a solution is obtained by inverting the stiffness matrix and this operation is the CPU-intensive operation. The displacement vector will be solved in the next stage. Contrary to the previous method, explicit methodology produces the result by solving the acceleration vector in the first stage. In this methodology, the mass matrix is considered as lumped. This process makes the computational process less intensive than implicit and time integration in implicit is unconditionally stable, whereas explicit time integration is not [18–20]. This condition happens because in explicit methodology, the constraint in terms of the critical step should be fulfilled. This situation ensures the explicit technique requires a much tinier time step and very tiny steps. Calculation and analysis of complex phenomenon that involves high non-linearity as well as requires tiny steps such as collision and grounding mean that the explicit technique is most suitable. The required calculation efforts are fewer than the implicit methods which mean the convergence of calculations is much easier to realize [21].

3 Physical experiment on ship material

In defining material for virtual simulation, realistic material model is needed to obtain robust results at the end of the simulation process. Properties of embedded material in simulation can be acquired from the experiments using the actual material on a ship's structure. Both destroyed and repair materials were applied to the side hull of the ship. The destroyed material from two materials which are presented in Figures 6 and 7 were tested and experimented on to acquire its material characteristics. The hardness test and chemical composition experiments were chosen to be performed for several reasons:

Table 1: Chemical composition experiment results.

Element	symbol	Composition		Unit	Difference	Unit
		General	Measured			
Iron	Fe	98.67-99.13	98.6000	%	0.07	%
Manganese	Mn	0.60-0.90	0.848	%	5.78	%
Carbon	C	0.27-0.34	0.29	%	7.41	%
Phosphorous	P	≤0.04	0.034	%	15.00	%
Sulfur	S	≤0.05	0.0954	%	47.59	%
Silicon	Si		0.0239	%		
Chromium	Cr		0.0059	%		
Molybdenum	Mo		0.0071	%		
Nickel	Ni		<0.0050	%		
Aluminium	Al		<0.0020	%		
Cobalt	Co		0.0133	%		
Cuprum	Cu		<0.0030	%		
Niobium	Nb		0.0078	%		
Titanium	Ti		<0.0020	%		
Vanadium	V		0.0055	%		
Wolfram	W		<0.0250	%		
Plumbum	Pb		<0.0100	%		
Calcium	Ca		0.0003	%		
Zirconium	Zr		0.0051	%		

Table 2: Hardness testing results.

Text Mode	Symbol	Hardness		Difference	Unit
		General	Measured		
Hardness Rockwell A	HRA		50.37		
Hardness Rockwell B	HRB	80	81.49	1.83	%
Hardness Vickers	HV	155	154.35	0.42	%
Hardness Brinell	HB	149	154.35	3.47	%

- *Hardness test*
  They are simple and inexpensive - ordinarily no special specimen need be prepared, and the testing apparatus is relatively inexpensive. The test is non-destructive - the specimen is neither fractured nor excessively deformed; a small indentation is the only deformation. Other mechanical properties often may be estimated from hardness data, such as tensile strength [16].
- *Chemical experiment*
  The composition of the material equals with the strength and other physical characteristics of the material. The changes in composition will affect the mechanical properties and simulation results. The chemical characteristics can be considered as a good comparison and a verification of the hardness test and also can be verified with the material's mechanical properties standards.

Hardness tests are performed using test method ASTM E18-05 ϵ^{-1} with test type Rockwell Hardness Number (HRA) load test 60 kgf [22]. As for chemical composition, the test is conducted using WAS/PMI-MASTER Pro spectrometer from Oxford Instruments [23].

The results and comparison with the predicted material of both tests are presented on Tables 1 and 2. The comparison of the material was performed only on destroyed material because the repair material had been confirmed used high-strength low-alloy class material AH36. Based on observation test result and reference of material characteristic [24], it was concluded that the sample of the destroyed material from the struck ship material was included in plain medium-carbon steel, type AISI 1030

Table 3: Material properties of destroyed material: medium-carbon steel 1030.

Properties	Symbol	Value	Unit
Density	ρ	7850	kg/m^3
Young's Modulus	*EX*	210	GPa
Poisson Ratio	*NUXY*	0.30	
Yield Strength	σ_Y	345	MPa
Ultimate Strength	σ_U	550	MPa

Table 4: Material properties of repair material: steel grade AH36.

Properties	Symbol	Value	Unit
Density	ρ	7850	kg/m^3
Young's Modulus	*EX*	200	GPa
Poisson Ratio	*NUXY*	0.29	
Yield Strength	σ_Y	350	MPa
Ultimate Strength	σ_U	490	MPa

specifically. Based on these results and conclusions, material properties for both destroyed and repair materials are presented in Tables 3 and 4 consecutively.

4 Numerical simulation

Collision simulations were performed for various physical parameters *i.e.* location penetrations and ship materials with the ANSYS LS-DYNA [25]. The struck and striking ships model was using the ships involved in a collision accident on the Sunda Strait between Java Island and Sumatra Island, Republic of Indonesia. The striking ship was a 144.5 m cargo reefer where the breadth of this ship was 19.8 m and height of ship was 10.2 m which was defined with rigid elements. The struck ship on the other hand was an 85.92 m Ro-Ro passenger where the breadth of this ship was 15 m, height of ship was 10.4 m and the double skin's widths was 2.5 m and 3.4 m which was defined as a deformable structure. In the numerical simulation, the actual material density of the proposed materials as mentioned in the previous section namely plain medium-carbon steel 1030 and steel grade AH36 were applied to the structural model so that the mass of model in the virtual experiment was defined as the mass of observed compartment models, such as the middle region compartment of the struck ship and fore end region of the striking ship.

$$\sigma_y = \left[1 + \left(\frac{\dot{\varepsilon}}{C}\right)^{\frac{1}{P}}\right]\left(\sigma_0 + \beta E_P \varepsilon_P^{eff}\right) \quad (1)$$

where σ_y is yield stress (Pa), ϵ is strain rate (s^{-1}), C is Cowper-Symonds strain rate parameters (s^{-1}), P is Cowper-Symonds strain rate parameters, σ_o is initial yield stress (Pa), β is hardening parameter, and ϵ_P^{eff} is effective plastic strain.

The two ship materials shown in Tables 3 and 4 were applied at the double side skin structure and were defined as plastic-kinematic material in the virtual experiment. The yield characteristic of this material is given in Equation 1. Three penetration locations were used as the location of the target point in this study as indicated in Figure 8. Location 1, represented contact on the hull region with the double skin width 3.4 m. Location 2, implied penetration point right on the transition position from double skin width 3.4 m to 2.5 m. Location 3 considered the contact point on the region with the double skin width 2.5 m.

In the virtual simulation, the striking ship moved with attached velocity 12 kts or 6.17 m/s to proposed target points while during the collision process, the displacement on the struck ship was set to be fixed at centerline with the ends of the model clamped. In the side ship model illustrated in Figure 8, the fixation was applied for the transverse frames and longitudinal girder in the end part of the structure model. At the end of side shell plating, axial displacements were restrained. The element choice for present research was Belytschko-Leviathan element. The element-length-to-thickness (ELT) ratio within the range of 5-10 was applied, especially into the deformable structure model of the struck ship so that the local stress and strain fields could be captured well. Fine mesh with size 80 mm was applied on the core area of the struck ship and fine mesh with size 90 mm and 100 mm were applied on the transition and the outside area respectively. The element-length-to-thickness (ELT) ratio for this area in range 8-10. The area of the rigid element of the striking ship model was divided into two parts: the first area would experience direct contact with the struck ship. A fine mesh with size 340 mm was applied at this area. The second was the rest area, where a fine mesh of size 680 mm was applied

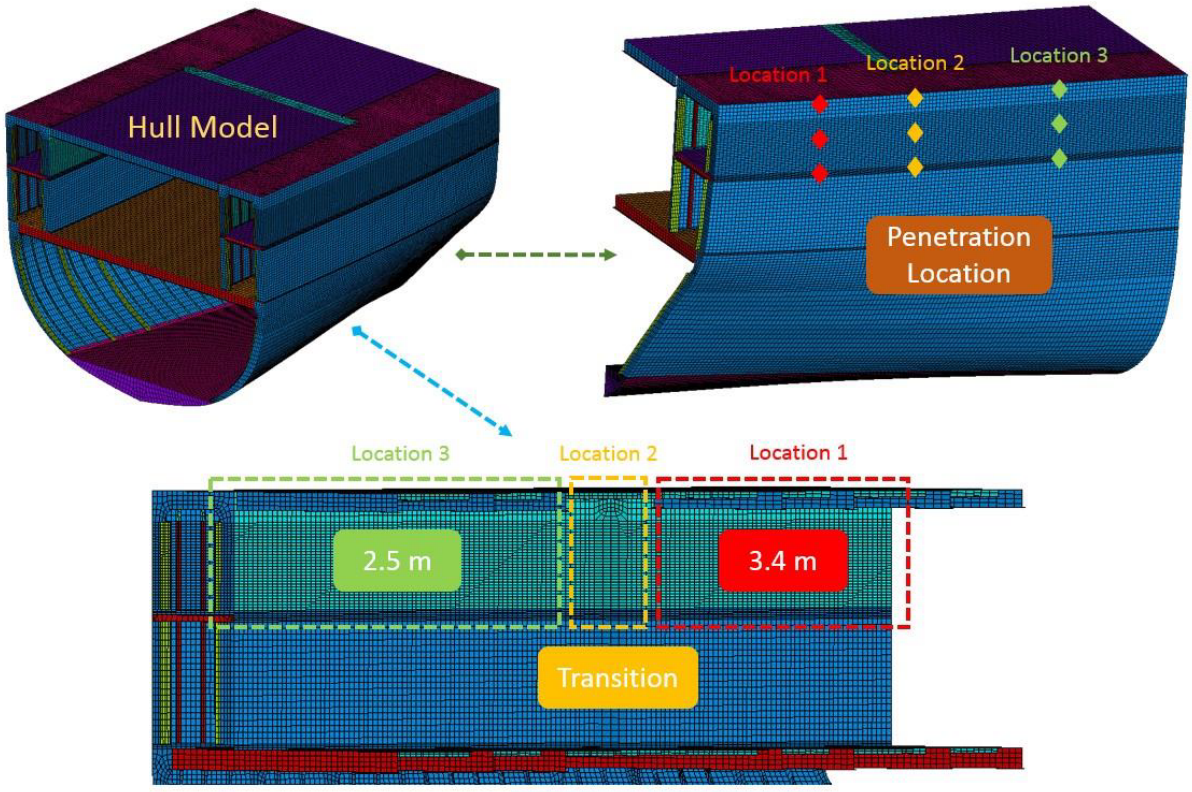

Figure 8: Penetration locations on struck ship DSS structure.

5 Observation on structural response

5.1 Global characteristic

The observation in this sub-section was performed on characteristic results globally. After dynamic collision simulations were performed, the calculation of finite element code showed the internal energy of the global phenomenon system. This energy was defined as the energy needed to plastically deform or even destroy the structure during the impact process. In this work, the terms of *energy* and *collision energy* refer to the terms of the virtual calculation results of internal energy. The trend line on collision energy as presented in Figure 9 indicated that the double skin structure (DSS) with wider width between outer and inner skin absorbed bigger energy in the collision process. In terms of ship materials, steel grade AH 36 produced bigger collision energy than medium-carbon steel 1030. The response of energy subjected to material was directly proportional with the mechanical properties especially the yield strength of destroyed and repair material. The difference between these two materials was not significant with the value below 1.5% and results also indicated the yield strength of these materials could be used to estimate the energy magnitude in the impact phenomenon process namely collision and grounding. The comparative graph for material response on all locations is presented in Figure 10. Besides direct analysis of the physical response, statistical results of the proposed scenario are also presented in Table 6. Collision energy and damage on DSS structure were taken as the main observation. The calculation of mean, median, mode and deviation standard were performed to obtain the conclusion regarding the data distribution. These calculations were intended to present the overall structural behaviour after collision happened on the middle region compartment. The more specific calculations, such as per impact location and applied material are presented in the Appendix.

Statistical analysis indicated that no significant differences in terms of proposed parameter responses were found. The result distribution in terms of damage to inner and outer skin was even under 0.5. The difference between sample and average value was very small and the diversity of all observed results was very low. The results also indicated that since the deviation standard was close to zero, the data points tend to be very close to the mean which also

Table 5: Thickness of structural components.

No.	Location	Structure Member	Thickness Value	Unit
1	Side Shell	Baseline - waterline 4	12	mm
		Waterlines 4 - 8	10	mm
		Waterline 8 - upper deck	10	mm
2	Deck Plate	Tank top	12	mm
		Wagon deck	15	mm
		Middle deck	8	mm
		Erection deck	8	mm
		Erection deck (edge)	12	mm
3	Girder	Center girder	12	mm
	(Tank Top)	Side girder	10	mm
		Floor	8	mm
4	Frame	Main frame	9	mm
		Web frame	10-19	mm
		Side stringer	4-125	mm
5	Beam - Girder	Center deck girder	10-12	mm
	(Wagon Deck)	Side deck girder	10-12	mm
		Strong beam	9-12	mm
		Deck beam	7	mm
6	Beam - Girder	Strong beam	9	mm
	(Middle Deck)	Deck beam	7	mm
7	Beam - Girder	Strong beam	7	mm
	(Erection Deck)	Deck beam	10-16	mm

called the expected value of the set. The difference in structural damage could be found in Locations 1, 2 and 3 which meant the structural arrangement and configuration significantly influenced damage on DSS structure, not only from materials effects. The shape factor was indeed influencing the damage in the contact process. However in the proposed model the shape of DSS structure was similar if it was compared to the fore end structure with curved shape. The statistical results also gave the indication of a relationship between energy and damage (displacement) on inner skin. Inner skin displacement was given the serious attention since the passenger cargo safety could be threatened and crushing material from passenger cargo could influence ship safety.

The tendency inclined that the higher energy was absorbed by the outer skin, the material of the inner skin would not displace farther than which outer skin absorbed less. The detailed statistical analyses are presented in Appendix A for location parameter and Appendix B for involved materials. More detailed characteristics of the inner skin after experiencing impacts at all proposed locations is presented in Table 7. The plastic strain of the inner skin and pressure extent by the end of the collision event are presented. As given in Table 7, the impact on

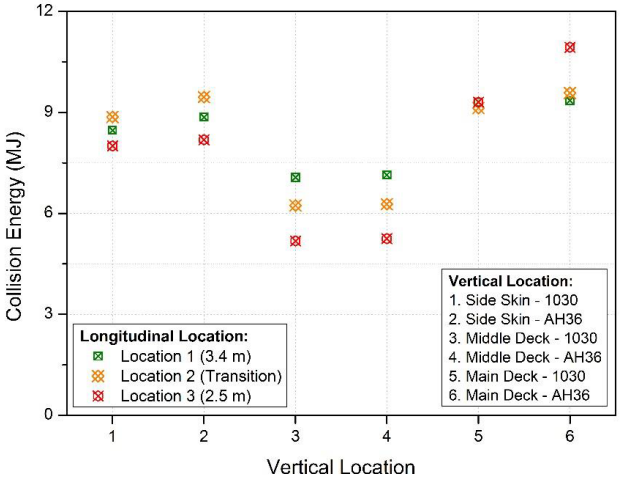

Figure 9: Global pattern of collision energy.

the shell at Location 2 or Transition produced the highest plastic strain which means the collision at this location caused skin plating to be more deformed than in other locations. The same result pattern was also obtained in terms of pressure. At the same location, produced pressure was the highest among all proposed locations.

Table 6: Statistical analysis of global results.

Location	DSS (m)	Analysis Order	Penetration Location	Material Type	Energy (MJ)	Outer Skin Damage (m)	Inner Skin Damage Displacement (m)	Inner Skin Damage Skin Status
Location 1	3.4 m	1	Shell	1030	8.4687	4.8040	0.6935	not breached
		2	Shell	AH36	8.8598	5.1498	0.6682	not breached
		3	Middle	1030	7.0648	4.7982	0.2499	not breached
		4	Middle	AH36	7.1428	4.7984	0.2499	not breached
		5	Main	1030	9.3020	4.4078	0.2499	not breached
		6	Main	AH36	9.3496	4.3921	0.4474	not breached
Location 2	Transition	7	Shell	1030	8.8664	4.8831	0.6043	tear formed
		8	Shell	AH36	9.4542	4.6447	0.7497	tear formed
		9	Middle	1030	6.2322	4.6835	0.2499	not breached
		10	Middle	AH36	6.2722	4.6835	0.2499	not breached
		11	Main	1030	9.1280	4.5045	0.2499	not breached
		12	Main	AH36	9.5761	4.4204	0.2530	not breached
Location 3	2.5 m	13	Shell	1030	8.0049	5.6869	0.2499	not breached
		14	Shell	AH36	8.1865	5.5705	0.2499	not breached
		15	Middle	1030	5.1835	4.4514	0.2499	not breached
		16	Middle	AH36	5.2502	4.4917	0.2499	not breached
		17	Main	1030	9.3020	4.3082	0.2499	not breached
		18	Main	AH36	10.9372	4.6426	0.4474	not breached
Mean					8.1434	4.7401	0.3674	
Median					8.6642	4.6641	0.2499	
Deviation Standard					1.6142	0.3858	0.1842	

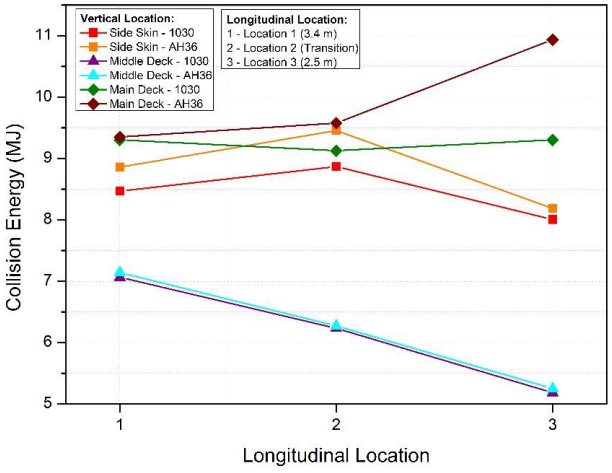

Figure 10: Material effect to energy magnitude after collision process.

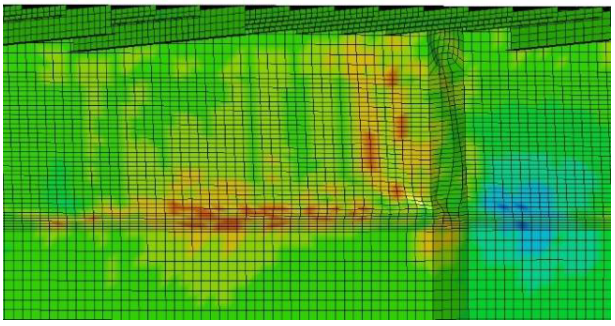

Figure 11: Pressure contour after collision at Location 1.

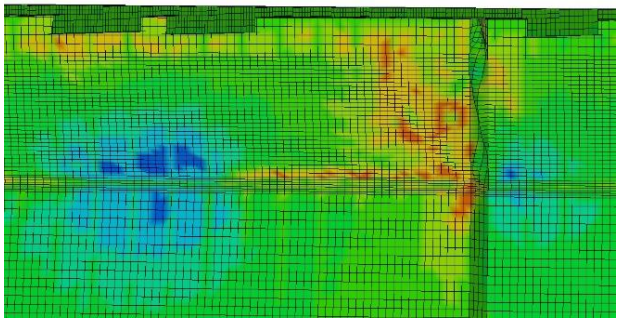

Figure 12: Pressure contour after collision at Location 3.

The results between collisions at shell and main deck were not significantly different if they were compared to results for the middle deck at three locations. The contour of all locations indicated that, after collision at the Locations 1 and 3, distribution of strain and pressure were not as remarkable as at the transition location. The contour illustration of three different locations is given in Figures 11-13. If bigger ships or a higher velocity collided with this ship at this specific location, the striking object was predicted to successfully penetrate the inner shell, which remarkable damage, especially at wagon deck was unavoidable.

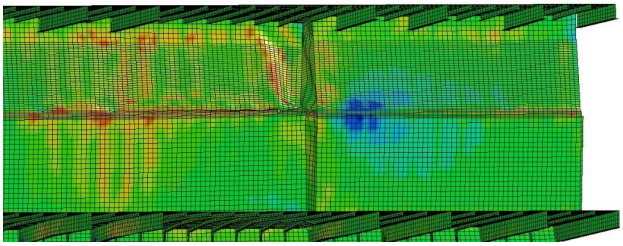

Figure 13: Pressure contour after collision at Location 2.

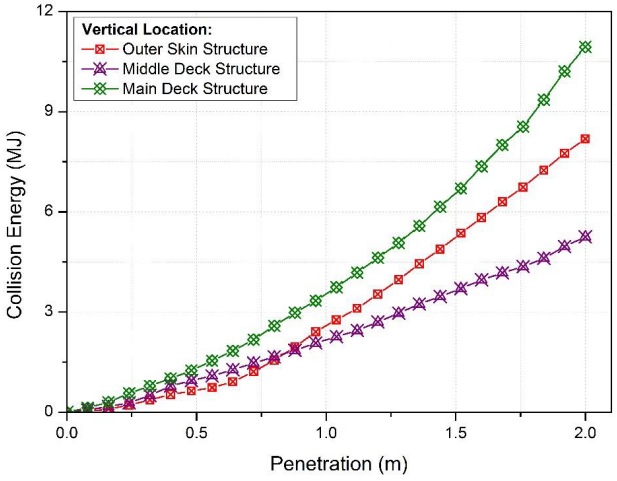

Figure 14: Energy pattern for different structure members.

The statement regarding the transition location in terms of strain and pressure would be sharpened during the discussion on damage comparison which is conducted in the next sub-section.

5.2 Structure response accounting for location of penetration

The arrangement and configuration of structural members, besides giving influence on energy magnitude due to its own, they also would give direct effect to its components. In this work, DSS structure of middle region compartments was divided into three main locations based on a vertical axis namely: outer skin, middle deck and main deck. A series of observations was performed on these locations after the striking ship penetrated the specific target point. As presented in Figure 14, three different structural components had different characteristic in terms of energy absorption. The middle deck, whose structure did not continue in transverse axis and connect with inner skin of DSS structure, produced a different pattern compared to the main deck. Energy magnitude after the collision process at this location was lower than in other locations because

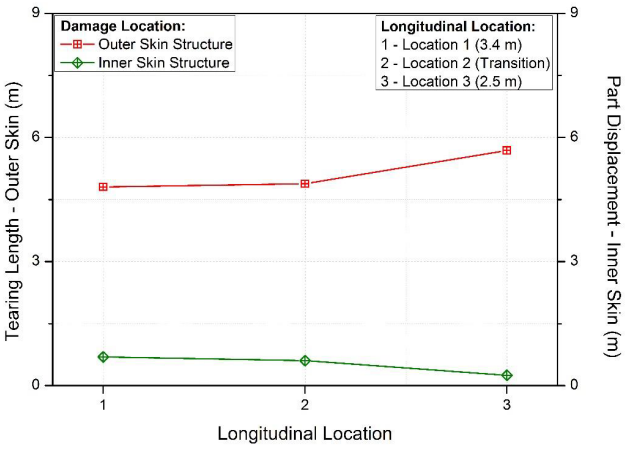

Figure 15: Comparative damage between outer and inner skin.

the structural members that could be destroyed were less than in other locations.

The collision at the main deck, which during and by the end of the collision process involved many more structural members, such as the main deck plate, strong beam, deck beam, outer skin, web frame, and main frame, than collisions at outer skin and middle deck, collision at the main deck also produced the highest energy compared to other locations. The less total structure members that could be destroyed during collision would directly affect the total destroyed material volume by the end of the collision process. The correlation between the energy and destroyed material also had been introduced by several researchers such as by Minorsky [7], Woisin [9], Zhang [3] and Bae *et al.* [26]. The collision at the main deck, which during and in the end of collision process at the main deck involved much structural member, such as main deck plate, strong beam, deck beam, outer skin, web frame, and main frame, than collisions at outer skin and middle deck produced highest energy than other locations.

5.3 Comparison on damage characteristic

In terms of damage, the size of DSS structure affected the damage on outer and inner skins. The location on this research, besides being divided by vertical direction, also was divided by longitudinal direction. On the longitudinal axis, the partition was performed according to width between outer and inner skin. Figure 15 represents the relation between DSS dimension and damage on its component subjected to the impact load. The graph indicated that the greater damage experienced by outer shell, less the inner skin structure would be displaced after collision process. The tendency on Figure 16 also shows that the big-

Table 7: Detail of inner skin after experienced impacts.

Location	DSS (m)	Analysis Order	Penetration Location	Material Type	Post-Impact Characteristic		
					Displacement (m)	Plastic Strain (-)	Pressure (Pa)
Location 1	3.4 m	1	Shell	1030	0.6935	1.20E−01	2.51E+08
		2	Shell	AH36	0.6682	1.20E−01	2.58E+08
		3	Middle	1030	0.2499	4.00E−02	2.11E+08
		4	Middle	AH36	0.2499	4.00E−02	2.14E+08
		5	Main	1030	0.2499	1.20E−01	2.51E+08
		6	Main	AH36	0.4474	1.20E−01	2.58E+08
Location 2	Transition	7	Shell	1030	0.6043	1.80E−01	2.48E+08
		8	Shell	AH36	0.7497	1.80E−01	2.91E+08
		9	Middle	1030	0.2499	4.00E−02	2.24E+08
		10	Middle	AH36	0.2499	4.00E−02	2.28E+08
		11	Main	1030	0.2499	6.00E−02	2.60E+08
		12	Main	AH36	0.2530	6.00E−02	2.68E+08
Location 3	2.5 m	13	Shell	1030	0.2499	1.00E−01	2.50E+08
		14	Shell	AH36	0.2499	1.00E−01	2.65E+08
		15	Middle	1030	0.2499	4.00E−02	2.28E+08
		16	Middle	AH36	0.2499	4.00E−02	2.32E+08
		17	Main	1030	0.2499	6.00E−02	2.61E+08
		18	Main	AH36	0.4474	6.00E−02	2.64E+08

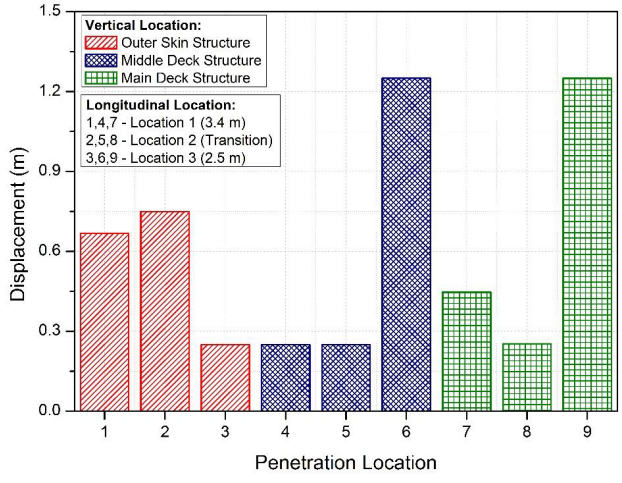

Figure 16: Displacement tendency of inner skin on 9 different locations.

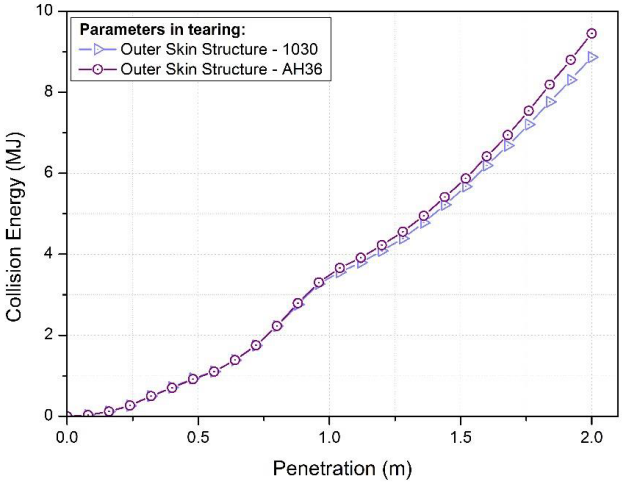

Figure 17: Energy pattern during hole formed in the end collision process.

ger the width between the two skins, the less the inner skin would experience displacement in a side collision.

After all collision simulations were conducted, two collision scenarios at transition zone (Location 2), a hole was formed in the inner skin and tearing damage was formed after the collision on the outer skin structure directly by the end of the collision process. The characteristics and condition of the inner shell still demand bigger concern even though the hole was not significantly formed and the striking ship did not breach the inner skin. Despite the hole size in the inner plating, with the current velocity, 12 kts had already able to form a hole in this zone. In future, if a collision occurs at this specific location, such as the transition zone, that involved a larger striking structure or a faster striking velocity, it was feared that the structure at this location would experience massive destruc-

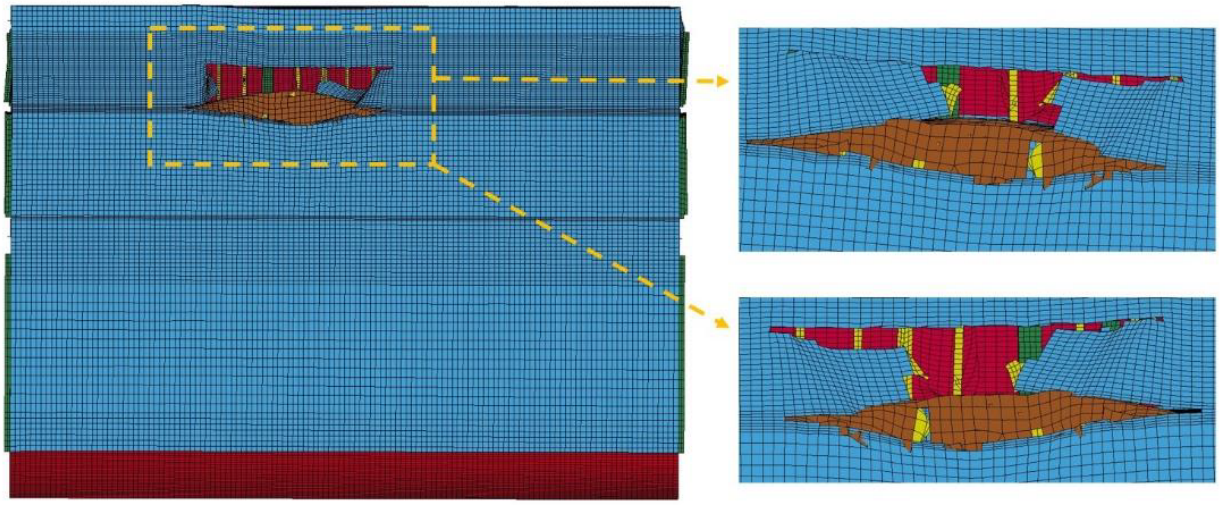

Figure 18: Deformation on DSS outer skin after collision on outer skin structure – 1.

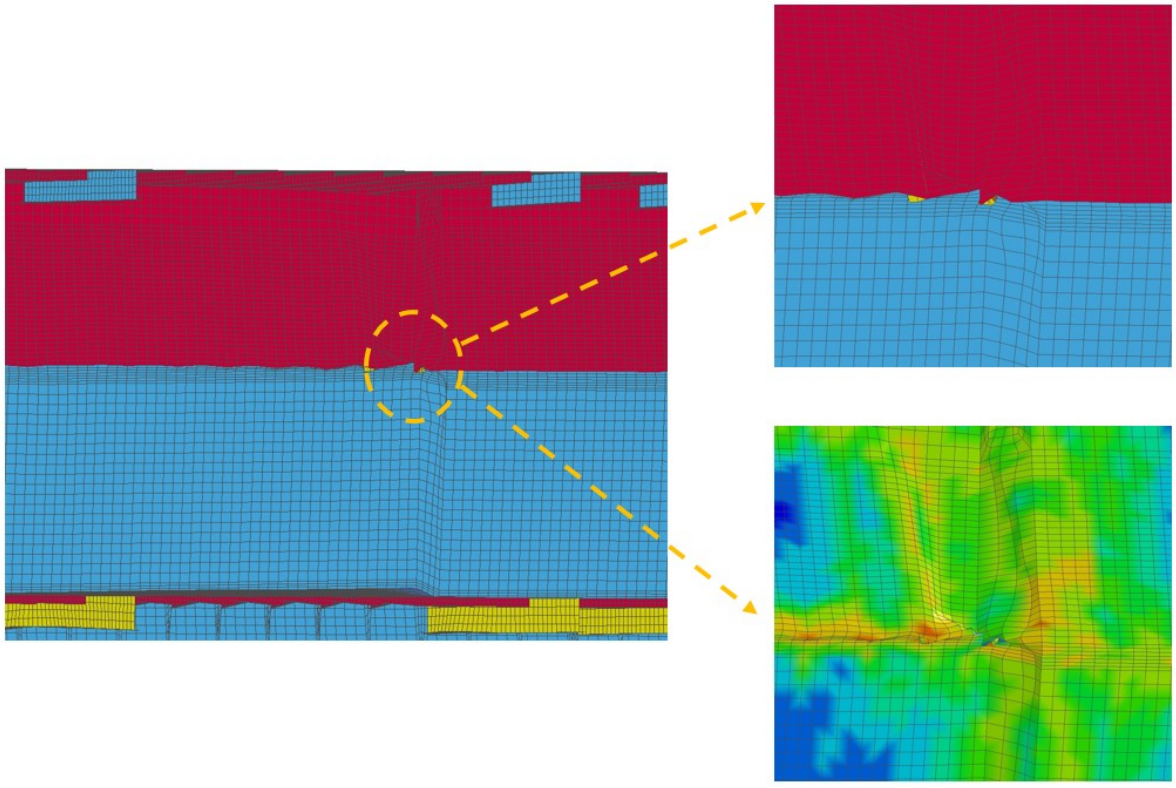

Figure 19: Deformation on DSS inner skin after collision on outer skin structure- 2.

tion. The results regarding damage characteristics in the present section could be considered to be in agreement with results in strain and pressure aspects as discussed in the previous sub-section.

The energy pattern and damage on this scenario are presented in Figures 17-19. The comparison of collision energy between destroyed material medium-carbon steel 1030 and repair material high-strength low-alloy steel grade AH36 is presented in Figure 14 and indicated that two applied materials had similar mechanical abilities during confronted accidental load. The substitution of side structure material during the repair process can be considered as a good preference in terms of material capability and performance.

6 Conclusion

A series of ship-to-ship collision analyses was presented in this paper. Physical experiments and tests of marine plate from involved ships in a side collision incident were performed to obtain material properties to support the numerical simulation process. Analyses by finite element approach were performed to produce virtual experiment data. Statistical analysis and direct observation on calculation results were presented in previous sections.

Distribution characteristics in statistical data described the variation data as very low which meant the results distribution did not have significant difference and big diversity. This condition could be considered to show good results since in the same structure model, the significant discrepancy of energy and damage were unlikely to be found. On the final results, several relationships between phenomena on double skin structure (DSS) were concluded and successfully verified by previous theory and methods from other researchers. For the ship with different DSS size and configuration it showed the collision on the transition zone could be classified as dangerous. In present research, after collision on outer skin structure, minor tearing damage was formed at the transition zone. Even though it was not significant, other situations and scenarios, such as the striking body being bigger and faster, remarkable damage on the side structure had a high probability to take place on the DSS structure.

The present analysis can be applied to different collision scenarios since the calculation and observation of ship collision can provide the behavior of structural components subjected to accidental load and be useful in improving structural reliability. This situation shows that the prediction of limitless collision scenarios is continuously needed with the advances in the development of structural safety. The analysis on collision with other parameters such as velocity can be considered a good opportunity for future work. Deployment of probability analysis by genetic algorithm and Bayesian network is encouraged by the authors.

Acknowledgement: Gratitude is offered to the colleagues of the authors, Mr. Irfan Taufiqurrahman and Mr. Teguh Fajar Basuki both of who are from PT Samudra Marine Indonesia (SMI) Cilegon Branch, West Java, Republic of Indonesia for giving the chance to perform surveys on the repair processes of ships which have experienced collision accidents and providing material specimens for experiments and tests.

References

[1] P. Rigo, E. Rizzuto, Analysis and Design of Ship Structure. Ship Design & Construction, Volume 1 by Thomas lamb (Editor), The Society of Naval Architects and Marine Engineers, New Jersey, United States: Chapter 18, 2004.

[2] T. Wierzbicki, J.C. Driscoll: Crushing damage of web girders under localized static load, J. Construct. Steel Research 33 (1995) 199-235.

[3] S. Zhang, The Mechanics of Ship Collisions, Ph. D. Thesis, Department of Naval Architecture and Offshore Engineering, Technical University of Denmark, Lyngby, Denmark, 1999.

[4] C.P. Ellinas, Mechanics of ship/jack-up collisions, J. Construct. Steel Research 33 (1995) 283-305.

[5] D.M. Bae, A.R. Prabowo, B. Cao, J.M. Sohn, A.F. Zakki, Q. Wang, Numerical simulation for the collision between side structure and level ice in event of side impact scenario, Lat. Am. J. Sol. Struct. 13 (2016) 2691-2704.

[6] C.G. Soares, Y. Garbatov, Reliability of maintained ship hulls subjected to corrosion and fatigue under combined loading, J. Construct. Steel Research 52 (1999) 93-115.

[7] V.U. Minorsky, An analysis of ship collision with reference to protection of nuclear power ships, J. Ship Research 3 (2) (1959) 1-4.

[8] H. Vaughan, Bending and tearing of plate with application to ship-bottom damage, J. Naval Architects 3 (1978) 97-99.

[9] G. Woisin, Design against collision, Schiff and Hafen 31 (2) (1979) 1059-1069.

[10] N. Jones, A Literature Survey on the Collision and Grounding Protection of Ships, Ship Structure Committee Report, SSC-283, 1979.

[11] J. Amdahl, Energy Absorption in Ship-Platform Impact, Norwegian Institute of Technology, Report No: UR-83-34, 1983.

[12] E. Samuelides, P.A. Frieze, Fluid-structure interaction in ship collisions, Mar. Struct. 2 (1989) 65-88.

[13] P.T. Pedersen, S. Valsgaard, D. Olsen, S. Spangenberg, Ship impacts: bow collisions, Int. J. Impact Eng, 13 (2) (1993) 163-187.

[14] P.T. Pedersen, Review and application of ship collision and grounding analysis procedures, Mar. Struct. 23 (2010) 241-262.

[15] A.R. Prabowo, D.M. Bae, J.M. Sohn, A.F. Zakki, Evaluating the parameter influence in the event of a ship collision based on the finite element method approach, Int. J. Tech. 4 (2016) 592-602.

[16] A.R. Prabowo, D.M. Bae, J.M. Sohn, B. Cao, Energy behavior on side structure in event of ship collision subjected to external parameters, Heliyon 2 (2016) e00192.

[17] A.R. Prabowo, D.M. Bae, J.M. Sohn, A.F. Zakki, B. Cao, J.H. Cho, Effects of the rebounding of a striking ship on structural crashworthiness during ship-ship collision, Thin-Walled Struct. 115 (2017) 225-239.

[18] A.R. Prabowo, D.M. Bae, J.M. Sohn, A.F. Zakki, B. Cao, Development in calculation and analysis of collision and grounding on marine structures and ocean engineering fields, J. Aqua. Mar. Bio. 5 (2017) 00116.

[19] A.R. Prabowo, D.M. Bae, J.M. Sohn, A.F. Zakki, B. Cao, Q. Wang, Anal;ysis of structural behavior during collision event accounting for bow and side structure interaction, Theo. App. Mech. Lett. 7 (2017) 6-12.

[20] A.R. Prabowo, D.M. Bae, J.M. Sohn, A.F. Zakki, B. Cao, Rapid prediction of damage on a struck ship accounting for side impact

scenario models, Open Eng. 7 (2017) 91-99.
[21] O. Ozguc, P.K. Das, N. Barltrop, M. Shahid, Numerical modelling of ship collision based on finite element codes, the 3rd International ASRAnet Colloquium, Glasgow, UK, 2006.
[22] W.D. Callister Jr., Material Science and Engineering, An Introduction, Seventh ed. John Wiley & Sons, Inc., NY, 2007.
[23] ASTM International, ASTM E18-15 Standard Test Methods for Rockwell Hardness of Metallic Materials, ASTM International, PA, 2006.
[24] Oxford Instruments Analytical, PMI-MASTER Pro Precise, Mobile Metal Analysis, Oxford Instruments, High Wycombe, UK, 2013.
[25] ANSYS, ANSYS LS-DYNA user's guide, ANSYS, Inc., Pennsylvania, US, 2017.
[26] D.M. Bae, A.R. Prabowo, B. Cao, A.F. Zakki, G.D. Haryadi, Study on collision between two ships using selected parameters in collision simulation, J. Mar. Sci. App., 15 (1) (2016) 63-72.

Appendix A

Table A.1: Statistical analysis on Location 1.

Location	DSS (m)	Analysis Order	Penetration Location	Material Type	Energy (MJ)	Outer S. Damage (m)	Inner Skin Damage Disp. (m)	Inner Skin Damage Skin Status
Location 1	3.4 m	1	Shell	1030	8.4687	4.8040	0.6935	not breached
		2	Shell	AH36	8.8598	5.1498	0.6682	not breached
		3	Middle	1030	7.0648	4.79818	0.2499	not breached
		4	Middle	AH36	7.1428	4.79838	0.2499	not breached
		5	Main	1030	9.3020	4.40775	0.2499	not breached
		6	Main	AH36	9.3496	4.39213	0.4474	not breached
Mean					8.3646	4.7250	0.4265	
Median					8.6642	4.7983	0.3487	
Mode					-	-	0.2499	
Minimum					7.0648	4.3921	0.2499	
Maximum					9.3496	5.1498	0.6935	
Deviation Standard					1.0283	0.2860	0.2115	

Table A.2: Statistical analysis on Location 2.

Location	DSS (m)	Analysis Order	Penetration Location	Material Type	Energy (MJ)	Outer S. Damage (m)	Inner Skin Damage Disp. (m)	Inner Skin Damage Skin Status
Location 2	Trans.	7	Shell	1030	8.8664	4.8831	0.6043	tear formed
		8	Shell	AH36	9.4542	4.6447	0.7497	tear formed
		9	Middle	1030	6.2322	4.6835	0.2499	not breached
		10	Middle	AH36	6.2722	4.6835	0.2499	not breached
		11	Main	1030	9.1280	4.5045	0.2499	not breached
		12	Main	AH36	9.5761	4.4204	0.2530	not breached
Mean					8.2549	4.6366	0.3928	
Median					8.9972	4.6641	0.2515	
Mode					-	-	0.2499	
Minimum					6.2322	4.4204	0.2499	
Maximum					9.5761	4.8831	0.7497	
Deviation Standard					1.5711	0.1609	0.2249	

Table A.3: Statistical analysis on Location 3.

Location	DSS (m)	Analysis Order	Penetration Location	Material Type	Energy (MJ)	Outer S. Damage (m)	Inner Skin Damage	
							Disp. (m)	Skin Status
Location 3	2.5 m	13	Shell	1030	8.0049	5.6869	0.2499	not breached
		14	Shell	AH36	8.1865	5.5705	0.2499	not breached
		15	Middle	1030	5.1835	4.4514	0.2499	not breached
		16	Middle	AH36	5.2502	4.4917	0.2499	not breached
		17	Main	1030	9.3020	4.3082	0.2499	not breached
		18	Main	AH36	10.9372	4.6426	0.4474	not breached
Mean					7.8107	4.8585	0.2828	
Median					8.0957	4.5671	0.2499	
Mode					-	-	0.2499	
Minimum					5.1835	4.3082	0.2499	
Maximum					10.9372	5.6869	0.4474	
Deviation Standard					2.2643	0.6071	0.0806	

Appendix B

Table B.1: Statistical analysis on destroyed material (1030).

Location	DSS (m)	Analysis Order	Penetration Location	Material Type	Energy (MJ)	Outer S. Damage (m)	Inner Skin Damage	
							Disp. (m)	Skin Status
Location 1	3.4 m	1	Shell	1030	8.4687	4.8040	0.6935	not breached
		3	Middle	1030	7.0648	4.7982	0.2499	not breached
		5	Main	1030	9.3020	4.4078	0.2499	not breached
Location 2	Trans.	7	Shell	1030	8.8664	4.8831	0.6043	not breached
		9	Middle	1030	6.2322	4.6835	0.2499	not breached
		11	Main	1030	9.1280	4.5045	0.2499	not breached
Location 3	2.5 m	13	Shell	1030	8.0049	5.6869	0.2499	not breached
		15	Middle	1030	5.1835	4.4514	0.2499	not breached
		17	Main	1030	9.3020	4.3082	0.2499	not breached
Mean					7.9503	4.7253	0.3386	
Median					8.4687	4.6835	0.2499	
Mode					-	-	0.2499	
Minimum					5.1835	4.3082	0.2499	
Maximum					9.3020	5.6869	0.6935	
Deviation Standard					1.4809	0.4125	0.1774	

Table B.2: Statistical analysis on repair material (AH36).

Location	DSS (m)	Analysis Order	Penetration Location	Material Type	Energy (MJ)	Outer S. Damage (m)	Inner Skin Damage	
							Disp. (m)	Skin Status
Location 1	3.4 m	2	Shell	AH36	8.8598	5.1498	0.6682	not breached
		4	Middle	AH36	7.1428	4.7984	0.2499	not breached
		6	Main	AH36	9.3496	4.3921	0.4474	not breached
Location 2	Trans.	8	Shell	AH36	9.4542	4.6447	0.7497	not breached
		10	Middle	AH36	6.2722	4.6835	0.2499	not breached
		12	Main	AH36	9.5761	4.4204	0.2530	not breached
Location 3	2.5 m	14	Shell	AH36	8.1865	5.5705	0.2499	not breached
		16	Middle	AH36	5.2502	4.4917	0.2499	not breached
		18	Main	AH36	10.9372	4.6426	0.4474	not breached
Mean					8.3365	4.7548	0.3961	
Median					8.8598	4.6447	0.2530	
Mode					-	-	0.2499	
Minimum					5.2502	4.3921	0.2499	
Maximum					10.9372	5.5705	0.7497	
Deviation Standard					1.8057	0.3817	0.1969	